Acta Cryst. (1977). A33, 399–408

Ferroelastic Phase Transitions in Lead Phosphate–Vanadate $Pb_3(P_xV_{1-x}O_4)_2$

BY E. SALJE AND K. IISHI*

Mineralogisches Institut der Technischen Universität, Welfengarten 1, *D*3 *Hannover, Germany (BRD)*

(*Received* 1 *November* 1976; *accepted* 4 *December* 1976)

The 'pure' ferroelastic behaviour of P-rich $Pb_3(P_xV_{1-x}O_4)_2$ is of the improper type. The ferroelastic phase transition is antiferrodistortive and accompanied by a second one at a lower temperature. The temperature range of the intermediate phase is approximately 20°C. At the transition points singularities of phonon spectra, dielectric and optical behaviour, and lattice constants are found. The Raman frequencies, the infrared absorption and reflexion spectra are given and interpreted on the basis of a mechanical and a rigid-ion lattice-dynamical model. From the results a critical mode is predicted at the boundary of the Brillouin zone (L in $R\bar{3}m$). Further, the Γ phonon becomes weak at the lower transition point. The normal coordinates of both modes give parallel and antiparallel deviations of Pb positions from the [111] axis of the rhombohedral $R\bar{3}m$ high-temperature phase.

Introduction

Ferroelasticity is one of the most important properties of $Pb_3(P_xV_{1-x}O_4)_2$ (Salje & Hoppmann, 1976). The ferroelastic phase transition is accompanied by an antiferroelectric transition for $Pb_3(VO_4)_2$. Only in the P-rich phases does ferroelasticity seem to be a 'pure' effect (Brixner, Bierstedt, Jaep & Barkley, 1973). Nevertheless structural data reveal that the elementary cell transforms during the transition at 180°C in $Pb_3(PO_4)_2$, and it can be assumed that similar transformations take place at the transitions of the other mixed crystals (Keppler, 1970). Hence the phase transformation is of the antiferrodistortive type. The order parameter of the phase transition is not the ferroelastic deformation vector. Ferroelasticity must be an improper effect even for $Pb_3(PO_4)_2$.

Tørres (1975) has found by group theoretical methods that the mechanism of the phase transition and hence the improper ferroelastic behaviour is correlated with one of two possible irreducible representations at the L point of the Brillouin zone. To understand this effect two questions have to be answered: Is the phase transition unique or do several transitions appear within a small temperature range? Is it possible to assume the critical behaviour of a single zone-boundary phonon?

We interpret the phonon spectra, the linear elastic constants and the dielectric tensor with the help of the force constants and the effective ionic charge of the crystal. For this purpose Raman, infrared absorption and reflexion and dielectric measurements have been made. Mechanical and rigid-ion models were used for the calculation.

Experimental

Crystals grown by the Czochralski method were used for experimental work. They show perfect cleavage perpendicular to the pseudo-hexagonal c_H axis. Only thin plates could be used for most of the experiments.

Samples were oriented optically for Raman measurements. Only normal scattering with polarization of incident and scattered light along the principal axes of the index ellipsoid in the high-temperature phase was performed. The experimental arrangement has been described (Salje, 1974). Heating of the crystals was achieved by mounting a small oven, with quartz windows, around the samples. The temperature was measured with a Ni–Cr/Ni thermocouple. As the crystals almost always show multidomain structures in the low-temperature phase the scattered light was polarized incompletely. The determination of the Raman tensor was possible only for some lines. In all phases a broadening of lines was observed. The minimum line width was 10 cm^{-1}. The spectral resolution was set to 5 cm^{-1}. Because of the broadening of the lines some phonons in the low-frequency region could not be resolved even at −196°C.

The effect of the large line width was much more pronounced in the infrared experiment. Here a commercial Beckman instrument was used. The spectral range examined was 200 to 3300 cm^{-1}. The spectral line width was below 5 cm^{-1}. Powder spectra were recorded for all chemical compositions. Reflexion measurements could be obtained with E parallel and perpendicular to c_H only for good quality P-rich phase. For this purpose the crystals were cleaved and polished. An Al plate served as a reference mirror.

Identical samples were examined in the far infrared region. A Polytec Fourier spectrometer was used in the range from 30 to 300 cm^{-1}. Powder spectra and reflexion measurements were made. The relative deviations between the different measurements were below 10%. The absolute values were less exact. Hence the maximum of reflectivity in the 1000 cm^{-1} band was fixed to be 80% and all other values were normalized with respect to this peak.

The dielectric constants were measured with a Kerr Wayne autobalance bridge B642. Both the capacitance

* On visit from Department of Mineralogical Sciences and Geology, Faculty of Literature and Science, Yamaguchi University, Japan.

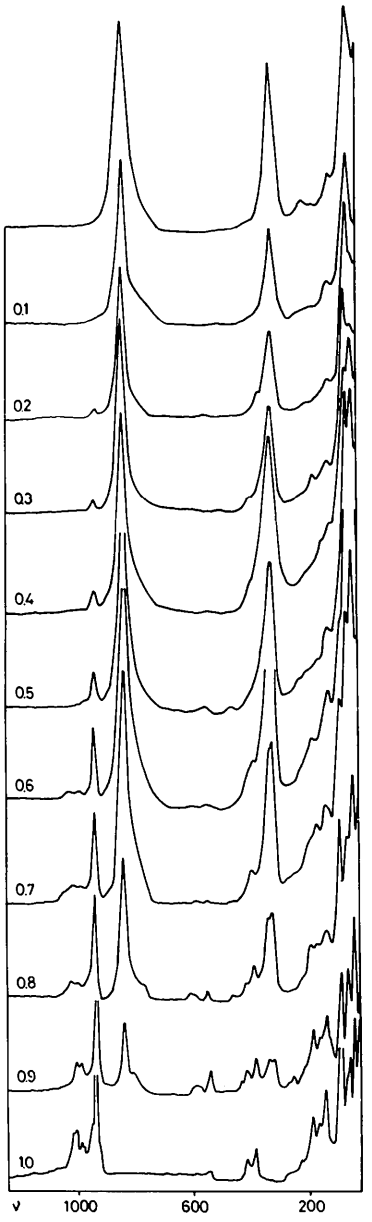

Fig. 1. Raman spectra of $Pb_3(P_xV_{1-x}O_4)_2$ for different x values (ν in cm^{-1}).

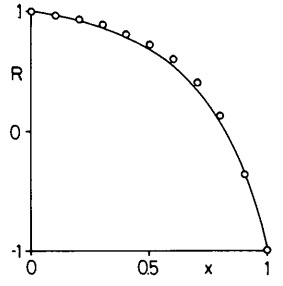

Fig. 2. Dependence of the intensity ratio R on chemical composition.

and the loss angle were measured. In the low-temperature region the loss angles were small and no corrections to the dielectric constant were necessary. The maximum error was below 5%. Above 80 °C the loss angle increases considerably. Here the differences between the samples were up to 30% for single crystals.

The X-ray work was done with a newly constructed high/low-temperature camera (Salje & Viswanathan, 1975). Focused Cu $K\alpha_1$ radiation was used. The resolution of the camera, after refinement, is better than 0·003 Å. For refinement all reflexions up to $2\theta = 70°$ were used. The samples had to be tempered to reduce the width of the line profiles. Above 150 °C the line width increases and the standard deviations became 4‰. In the trigonal high-temperature form the individual reflexions become sharp just after the phase transition.

Results

(*a*) *Spectroscopic*

The Raman spectra of powdered $Pb_3(P_xV_{1-x}O_4)_2$ specimens are shown in Fig. 1. It can be seen that in the high-frequency region (above 200 cm^{-1}) most of the lines are given by the nominal content of PO_4 and VO_4 complexes. The spectra can be interpreted in this region as a superposition of the tetrahedral lines with nearly no line shift with chemical composition. For comparison of the intensities of different scattering signals the ratio of the intensities of the 928 and 833 cm^{-1} lines is given in Fig. 2. These lines are the ν_1 phonon states of PO_4 and VO_4 respectively. Neglecting any interaction between the two phonons the theoretical depencence on chemical composition is

$$R = (I_{PO_4} - I_{VO_4})/(I_{PO_4} + I_{VO_4}) = \left[1 - x\left(\frac{\alpha_V + \alpha_P}{\alpha_V}\right)\right] \Big/ \left[1 + x\left(\frac{\alpha_V - \alpha_P}{\alpha_V}\right)\right].$$

The ratio of the polarizabilities $\alpha_P/\alpha_V = 0{\cdot}2$ as determined from the experimental values. From the excellent agreement between the experimental and theoretical curves in Fig. 2 it was concluded that the coupling between the two energy levels is negligible.

Polarized Raman spectra were taken with three different samples. For $x = 0{\cdot}9$ the spectrum is given in Fig. 3. In all experiments with polarized radiation depolarization was observed because of scattering at domain boundaries. In extreme multidomain scattering crystals almost no polarization was noticeable. The best polarization ratio was found to be 60%. Hence a separation of different B_g modes was impossible. Only the A_g (α_{zz}) were identified and these are present in Table 1.

To measure the thermal dependence of the Raman scattering the same samples were used. Fig. 4 shows that no soft-mode behaviour occurs. Some lines cannot be found in the high-temperature phase. Only a few phonons show a slowing down of their frequencies for some wavenumbers. As not all lines are really resolved

Table 1. *Observed phonon frequencies* (cm^{-1}) *at room temperature*

$Pb_3(VO_4)_2$	$Pb_3(P_{0.5}V_{0.5}O_4)_2$	$Pb_3(PO_4)_2$
IR (Powder)		
1050?	1055	1061
999?	985	1008
	920	975
856	850	925
(815)	(820)	
775	770	790
(660)	(660)	
570	575	
540	545	548
360	370	
345		
308	310	
175	200	220
140		160
100	130	120
Raman (Powder)		
	36·8	37·5 (Z)
	54·2	52·7
		58·6
	85	84·7 (Z)
113·5	121	123·7
	155	137·7 (Z)
		156·2
	186	183·6
		218
318·5	382	380·2
		385·0
		408·5
		409·9
	530	537·2
		598·3
765	760	930·8 (Z)
826·7	826·7	958·0
	931	983·2
	990	998

in the low-temperature phase it is likely that some further lines may shift. Nevertheless the spectral distributions of the different bands do not change much with temperature.

In some of the samples an additional peak with extremely low intensity was observed near 25 cm^{-1}. This peak could not be identified and was not taken into account in theoretical considerations. It is possible that it is due to impurities.

From the temperature dependence of the intensity of the 84 cm^{-1} line not one but two discontinuities at 160°C ($x=1$) are noticeable. These temperatures depend somewhat on the history of the crystal. The scattering signals are slightly broadened within the interval between the two transition points.

Measurements in the near infrared region were performed at room temperature (Fig. 5). The oscillator strengths are independent of PO_4–VO_4 couplings. Shifts of the absorption peaks with composition are given in Fig. 6. Here also the effect of line-shift is small and comparable with the results of the Raman scattering experiments. A powder spectrum of $Pb_3(VO_4)_2$ has been published recently (Baran, Botto & Aymonino, 1976). It is identical with ours but does not show the small peaks at 999 and 1050 cm^{-1}. This effect may be due to decomposition during crystal growth. From theoretical considerations we believe the spectrum of Baran *et al.* (1976) to be correct.

Reflexion measurements were made for $x=1$ and $x=0{\cdot}9$ at room temperature (Fig. 7). From these

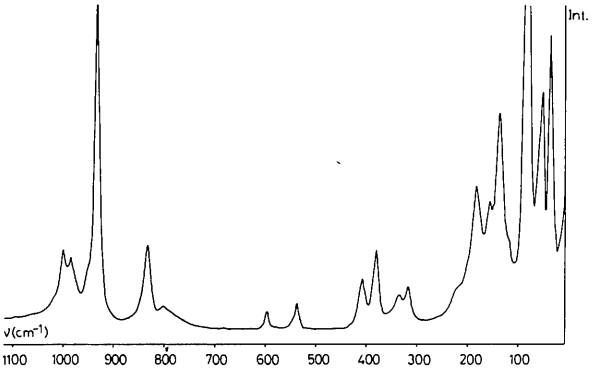

Fig. 3. Raman spectrum (α_{zz}) of $Pb_3(P_{0.9}V_{0.1}O_4)_2$.

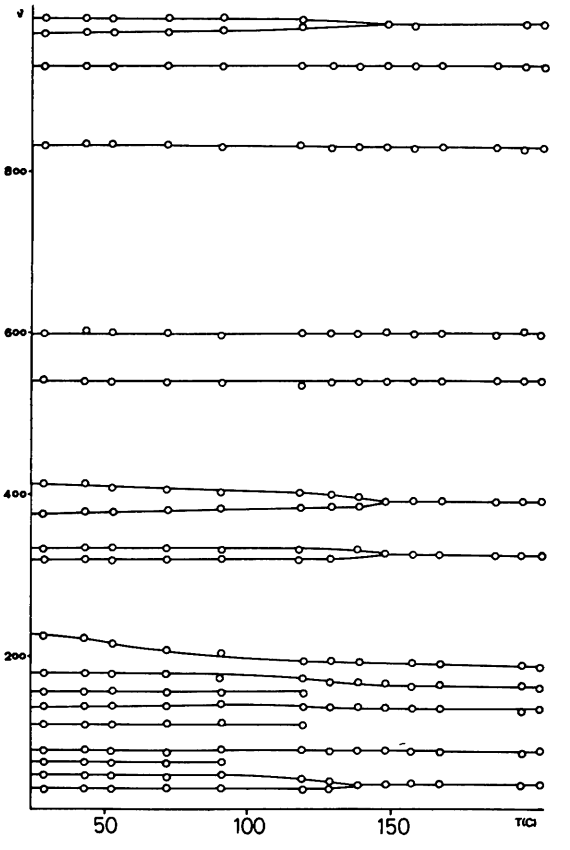

Fig. 4. Thermal dependence of Raman lines for $Pb_3(P_{0.9}V_{0.1}O_4)_2$.

experiments the different A_u and E_u modes (as a superposition of B_u modes) can be separated if the line-shifts

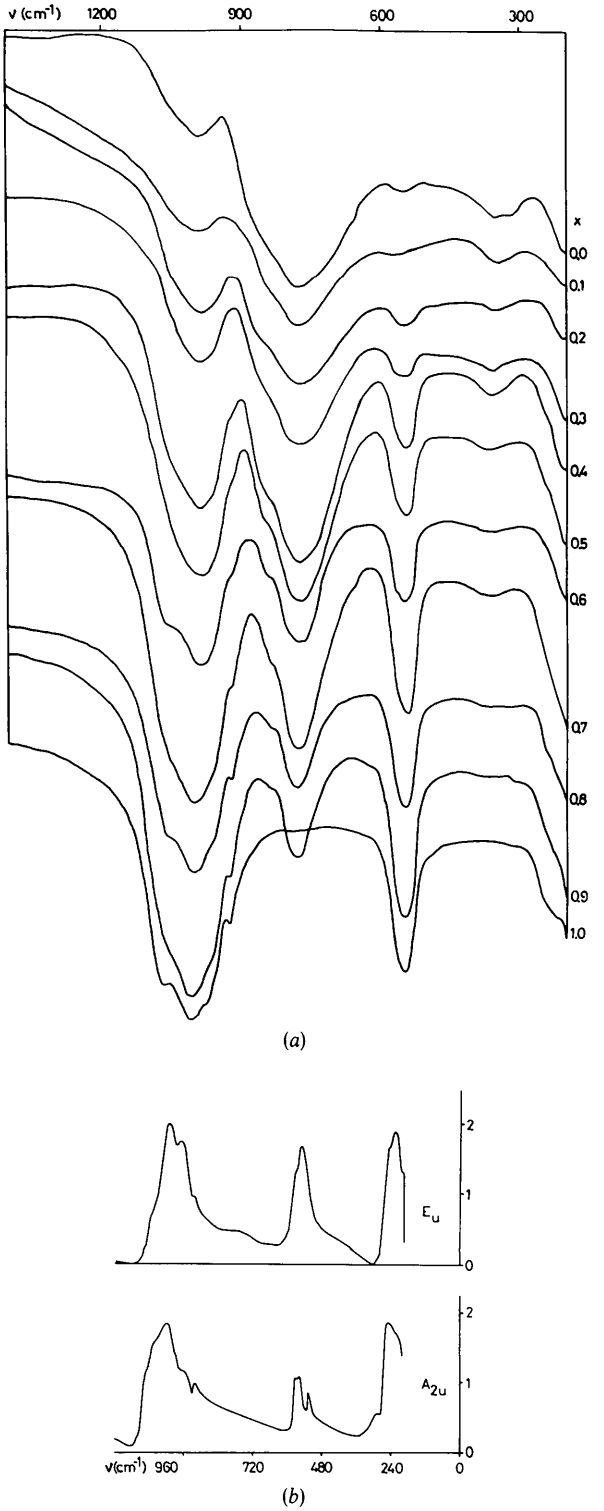

Fig. 5. Infrared spectra of powders $Pb_3(P_xV_{1-x}O_4)_2$ (*a*) and reflection spectra of $Pb_3(PO_4)_2$ single crystals (*b*).

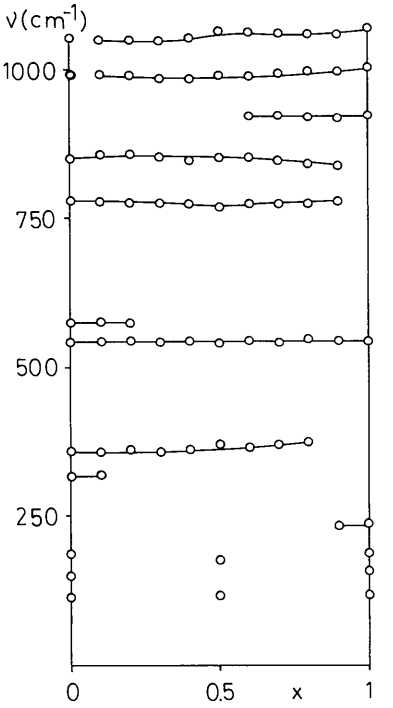

Fig. 6. Dependence of the strongest infrared absorption lines on chemical composition.

during the phase transitions are small; the pseudo-hexagonal polarization behaviour can be observed in the room temperature phase. To interpret the spectra a Kramers–Kronig analysis was attempted. The formula fitted was:

$$\varepsilon' = n^2 - \kappa^2 = \varepsilon_\infty + \sum_i \Delta\varrho_i \nu_i \frac{\nu_i^2 - \nu^2}{(\nu_i^2 - \nu^2) + \gamma_i^2 \nu^2}$$

$$\varepsilon'' = 2n\kappa = \sum_i \Delta\varrho_i \nu_i \frac{\gamma_i \nu}{(\nu_i^2 - \nu^2)^2 + \gamma_i \nu^2}$$

$$R = \frac{(n-1)^2 + \kappa^2}{(n+1)^2 + \kappa^2}$$

$$= \frac{(\varepsilon'^2 + \varepsilon''^2)^{1/2} + 1 - [2(\varepsilon'^2 + \varepsilon''^2)^{1/2} + 2\varepsilon']^{1/2}}{(\varepsilon'^2 + \varepsilon''^2)^{1/2} + 1 + [2(\varepsilon'^2 + \varepsilon''^2)^{1/2} + 2\varepsilon']^{1/2}}.$$

The damping constant γ and oscillator strength ϱ were fitted by trial and error. The different B splits were neglected to find the best solution for the phonon branches in the trigonal symmetry. The resulting frequencies of the longitudinal and transverse modes are presented in Table 4.

Reflexion measurements as well as powder absorption spectra were made in the far infrared region. The additional *TO* modes from powder spectra are incorporated in Table 4. The observed reflexion spectra could not be fitted by a Kramers–Kronig analysis. This effect is due to incorrect absolute values of reflectivity and spectral dependence of the Fourier detector.

Hence the longitudinal branches could not be determined in this spectral range.

(b) Dielectric constant

The dielectric constant for $Pb_3(PO_4)_2$ was determined along and perpendicular to c_H: $\varepsilon^{\parallel}=27$ and $\varepsilon^{\perp}=43$. The dielectric constant of the powder is 38 (Isupov, Krainik & Kasenko, 1973). Measurements on $Pb_3(VO_4)_2$ gave the same results as Gene, Dudnik & Singakov (1975): $\varepsilon^{\parallel}=38$ and $\varepsilon^{\perp}=49$. In the phosphate the loss angle was small up to approximately 140°C and increased with increasing temperature. The transition of the high-temperature phase is accompanied by a small step in the dielectric constants reported by Isupov *et al.* (1973). In single crystals this discontinuity is somewhat sharper. Near 160°C the curve of $Pb_3(PO_4)_2$ starts to increase with temperature but no singularity occurs.

The high-temperature dielectric constants can be taken from the refractive indices given by Tørres, Aubree & Brandon (1974). At room temperature $\varepsilon^{\infty}_{xx}=4{\cdot}203$, $\varepsilon^{\infty}_{yy}=4{\cdot}285$, and $\varepsilon^{\infty}_{zz}=4{\cdot}097$. The spontaneous deformation part $\varepsilon^{\infty}_{xx}-\varepsilon^{\infty}_{yy}$ vanishes near the transition point. Between 160 and 180°C the domain pattern appears in thin plates. The domain walls are at 60° to each other and symmetric to the ferroelastic domains (Salje & Hoppmann, 1976). Some Czochralski-grown virgin crystals do not exhibit the domains first. If these crystals are pressed to induce the ferroelastic domains and heated several times through the transition points the domains of the intermediate phase can be observed for thin plates.

(c) Lattice constants

The lattice constants show a significant thermal dependence (Fig. 7). In the monoclinic phase a and c increase, but b shows a thermal anomaly and shrinks with temperature. The expansion coefficients are approximately constant up to the phase transition at 180°C for a and c. The monoclinic angle shows little change with temperature. Above 160°C the reflexions hkl ($k=2$) and 404 become diffuse whereas all those lines remaining practically unchanged during the trigonal phase transition remain sharp. The reflexions 020, 404, 224, 620, and 424 are extremely broadened and could not be used for refinement of the lattice constants. The shrinkage of b induces lattice deformations observable as a line broadening of $h2l$ reflexions within the intermediate phase.

At the high-temperature phase transition the cell transformations are

$$a_H=b_M$$

$$b_H=\tfrac{1}{2}(b_M^2+c_M^2)^{1/2}$$

$$c_H=\tfrac{1}{2}[9a_M^2+c_M^2-6a_Mc_M\cos(180^\circ-\beta)]^{1/2}.$$

This formula is used to obtain the cell dimensions in Fig. 7. The values at room temperature and at 220° are compared in Table 2. They are different from those given by Ng & Calvo (1975), but agree with Keppler (1970).

Table 2. *Lattice constants of* $Pb_3(PO_4)_2$

T (°C)	a (Å)	b (Å)	c (Å)	β (°)
20	13·813 (5)	5·693 (1)	9·436 (3)	103·39 (3)
220	5·547 (2)	5·547 (2)	20·333 (7)	hexagonal

A further small discontinuity in b, well outside experimental error, was observed near 90°C (Fig. 7). Unfortunately no confirmation could be found by other methods. The reason for this thermal behaviour is not clear at present, but the transition can be anticipated from the phase diagram given by Hodenberg, Salje, Recker, Walraffen & Eckstein (1977).

(d) Lattice dynamics

An attempt to understand the ferroelastic behaviour of the crystals may be made in terms of lattice-dynamical model. This model has to explain the phonon frequencies, the dielectric constants, and also the elastic constants given by Cao-Xuan, Hauret & Chapelle (1975). To discover the reason for the phase transition, a critical parameter in this model must be correlated with the structural collapse.

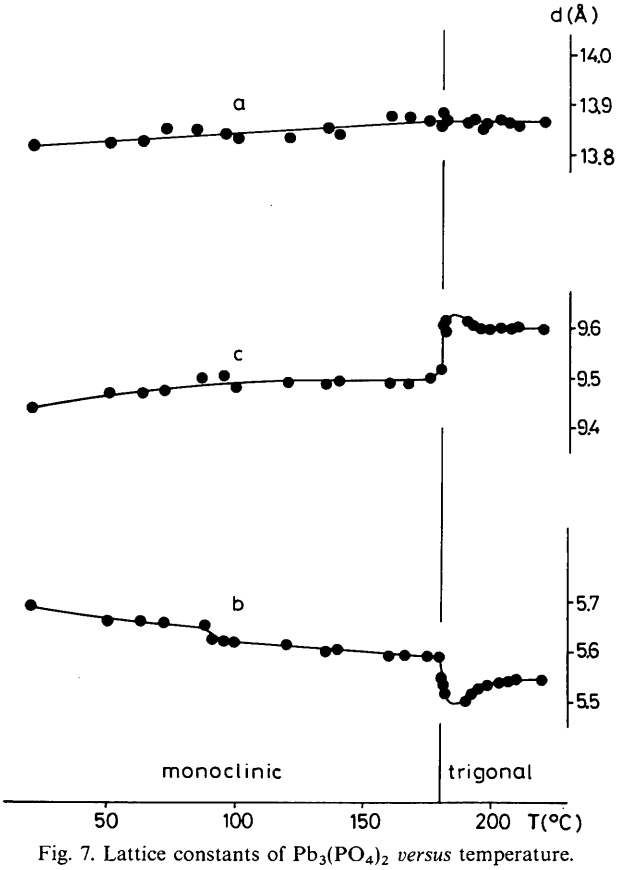

Fig. 7. Lattice constants of $Pb_3(PO_4)_2$ *versus* temperature.

In the present study the normal coordinate treatments were performed in two steps, those based on the short-range interaction model (SRM) and on the rigid-ion model (RIM). A modified Urey–Bradley force field was applied to the intramolecular vibrations of the phosphate complex. Correction terms were introduced for the intramolecular tension (κ) and the bond–bond interaction (p). A central force field was used intramolecular vibrations. The parameters used are given in Table 3.

Table 3. *Potential distribution for elastic constants*

Force constant	C_{11}	C_{33}	C_{44}	C_{66}	C_{12}	C_{13}	C_{14}
K	1	2	0	0	1	1	0
k_1	16	1	3	1	25	8	4
k_2	7	0	57	11	4	0	53
k_3	0	24	0	0	0	5	5
k_4	69	2	6	87	57	25	37
k_5	7	69	26	0	12	59	5
H	0	0	5	0	0	1	2
F	1	1	4	0	1	0	2
κ	0	0	1	0	0	1	0

To extend this model to the long-range forces, a Coulomb part was added to the dynamical matrix (Born & Huang, 1954):

$$D_{ij}^{C}(KK',\mathbf{y}\to 0)=Z_K e^2(m_K m_{K'})^{1/2}\{4\pi v^{-1}\lim_{\mathbf{y}\to 0}(y_i y_j/|\mathbf{y}|^2)$$
$$-Z_{K'}Q_{ij}(KK',\mathbf{y}\to 0)+\delta_{KK'}\sum(K'')Q_{ij}(KK'',\mathbf{y}\to 0)\}$$
$$\mathbf{D}=\mathbf{D}^S+\mathbf{D}^C;\ \mathbf{D}^C=Z'CZ.$$

The non-Coulomb part $\mathbf{D}^S$ was assumed to be the same as that used in SRM. The Coulomb coefficients $\mathbf{V}_{ik}(KK')$ were calculated by the Ewald (1921) method. Z means the tensor of effective ionic charge.

The force constants were least-squares fitted to the experimental phonon frequencies. From the SRM the elastic constants were calculated by the method of Shiro & Miyazawa (1971). The energy distribution of the elastic constants was also calculated (Table 3). It can be seen that only the Pb–O potential is responsible for the elastic behaviour of $Pb_3(PO_4)_2$. The elastic constants C_{11}, C_{33}, C_{66}, and C_{13} are given by the Pb(II)–O interaction (k_3,k_4,k_5) whereas C_{44}, C_{14}, and C_{12} are due to all Pb–O force constants. The agreement between the theoretical values and the experimental results is quite good for the transverse phonon branches and the elastic constants (Table 4). The *TO–LO* splitting and the dielectric constants cannot be calculated using the SRM. With the RIM the experimental data can be explained self-consistently. The effective ionic charges for the best fit are $Z_{Pb}=1{\cdot}4$, $Z_P=1{\cdot}7$, and $Z_O=-0{\cdot}7$ e. Typical values of O are in the range $-1{\cdot}2$ to $-1{\cdot}5$ e for highly ionic interactions. Hence the character of the bond within the PO_4 complex can be estimated to be 60% ionic.

The coupling of Pb with the PO_4 complexes is characterized by the rather high effective ionic charge Z_{Pb}. The influence of this parameter on the different phonon branches can be seen from the potential energy distribution matrix in Table 5. Here the lowest phonon

Table 4. *Observed and calculated data for* $Pb_3(PO_4)_2$

Mode	Exp.	SRM	RIM
A_{1g}			
ν_3	992	1010	1016
ν_1	928	929	930
ν_4	600	566	594
T'	166	186	184
T'	84	60	82
E_g			
ν_3	992	989	1001
ν_4	537	548	550
ν_2	390	392	381
R'	200	214	203
T'	140	106	109
T'	48	52	58
A_{2u}			
ν_3	995–1077	1010	1014–1034
ν_1	920– 927	929	930– 930
ν_4	557– 577	567	560– 578
T'	180 —	200	167– 240
T'	120 —	96	110– 115
E_u			
ν_3	980–1052	989	1001–1022
ν_4	540– 587	548	523– 539
ν_2	– –	394	406– 406
R'	215– 265	220	209– 230
T'	90– 185	115	91– 178
T'	55– 58	59	55– 61
$\varepsilon_0^{\perp}$	43		
$\varepsilon_0^{\parallel}$	27		
C_{11}	7·5	7·7	
C_{33}	9·1	9·6	
C_{44}	2·2	1·0	
C_{66}	1·1	1·5	
C_{12}	5·2	4·1	
C_{13}	2·8	2·7	
C_{14}	−0·2	−0·13	
K		5·05	5·8
k_1		0·45	0·53
Pb(I)—O 2·6232 Å k_2		0·04	0·05
Pb(I)—O 3·2133 Å k_3		0·67	0·92
Pb(II)–O 2·3734 Å k_4		0·30	0·15
Pb(II)–O 2·8289 Å k_5		0·14	0·04
Pb(II)–O 2·9449 Å			
H		0·24	0·21
F		0·51	0·37
κ		0·65	0·42
P		0·25	0·18
Z_{Pb}		0	1·4
Z_P		0	0·7
Z_O		0	−0·7

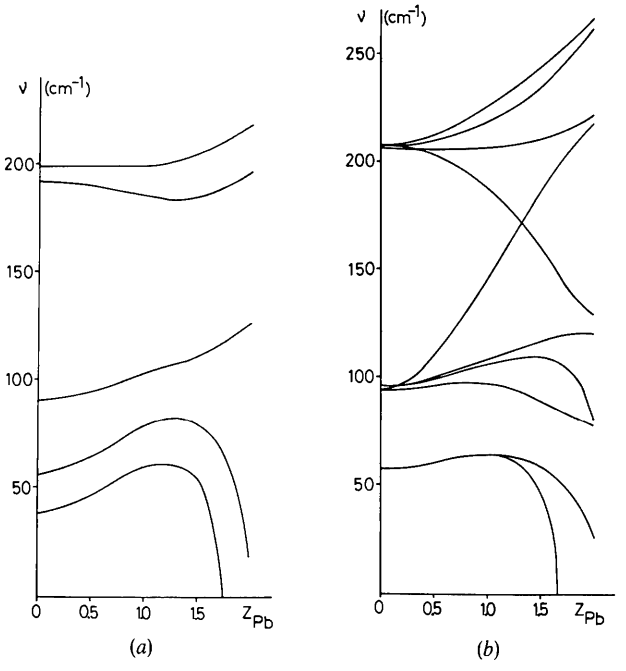

Fig. 8. Dependence of phonon frequencies on effective ionic charges. (*a*) E_u, (*b*) A_{2u}.

branch is mainly affected by small changes of Z_{Pb}. An increase of this effective ionic charge up to 1·6 e causes a critical slowing down of this phonon branch at the zone centre. In Fig. 8 the dependence of all phonon frequencies on this parameter is shown. The behaviour of the 48 cm^{-1} mode is typical for the structural phase transition caused by dynamical phenomena.

All calculations were performed for phonons with zero wavenumber. From the results of Tørres (1975) zone-boundary (L) modes can be expected to behave critically. Hence only the amplitudes and not the phases can be taken from our dynamical model. The amplitudes must be compared with the difference structure of both phases at the high-temperature transition point. In Figs. 9 and 10 both sets of deformation vectors are shown.

During the phase transformation both Pb positions shift parallel from the c_H axis towards b_M. The PO_4 complexes are somewhat rotated. The phases of the normal coordinates are changed relative to the deformation vectors. The lower-temperature transition shows an antiparallel shift of the two Pb atoms in phase with the normal coordinates calculated. The amplitudes of the deformation vectors in both sets increase continuously with decreasing temperature.

Table 5. *Potential energy distribution matrix*

		K	k_1	k_2	k_3	k_4	k_5	H	F	κ	P	Z
ν_3		101	0	0	3	0	0	3	3	3	−3	−10
ν_1		71	1	0	3	0	0	0	18	0	7	0
ν_4		3	11	0	5	0	0	20	18	18	0	25
T'		1	34	0	50	1	4	2	1	2	0	4
T'		5	2	0	96	3	12	2	3	2	0	−26
ν_3		102	0	0	0	0	0	4	3	3	−3	−9
ν_4		4	0	1	0	3	0	23	21	21	0	28
ν_2		0	17	1	0	7	0	45	32	−13	0	11
R'		0	64	6	0	15	1	2	2	−1	0	11
T'		0	8	16	0	37	7	3	2	0	0	26
T'		1	2	2	0	178	3	2	2	1	0	−90
ν_3	T	102	0	0	4	0	0	3	3	3	−3	−12
	L	97	0	0	4	0	0	3	3	3	−3	−7
ν_1	T	71	1	0	3	0	0	0	18	0	7	0
	L	71	1	0	3	0	0	0	18	0	7	0
ν_4	T	1	12	0	5	0	0	24	19	21	0	17
	L	4	12	0	4	0	0	21	19	19	0	21
T'	T	2	94	0	51	2	5	0	0	0	0	−55
	L	3	29	0	34	1	3	3	1	2	0	23
T'	T	1	16	0	68	2	7	0	0	0	0	5
	L	0	51	0	28	1	3	0	0	0	0	18
ν_3	T	102	0	0	0	0	0	3	3	3	−3	−9
	L	97	0	0	0	0	0	4	2	3	−3	−4
ν_4	T	4	0	1	0	3	0	26	23	23	0	20
	L	7	0	1	0	4	0	23	22	20	0	23
ν_2	T	0	15	1	0	5	0	40	28	−12	0	22
	L	0	15	1	0	5	0	40	28	−12	0	22
R'	T	0	70	3	0	15	1	3	2	−1	0	8
	L	1	48	0	0	22	0	3	2	0	0	23
T'	T	0	21	50	0	52	8	1	0	0	0	−33
	L	0	15	13	0	3	4	1	1	1	0	62
T'	T	0	10	9	0	211	7	6	4	−2	0	−145
	L	0	29	38	0	68	1	3	2	−1	0	−40

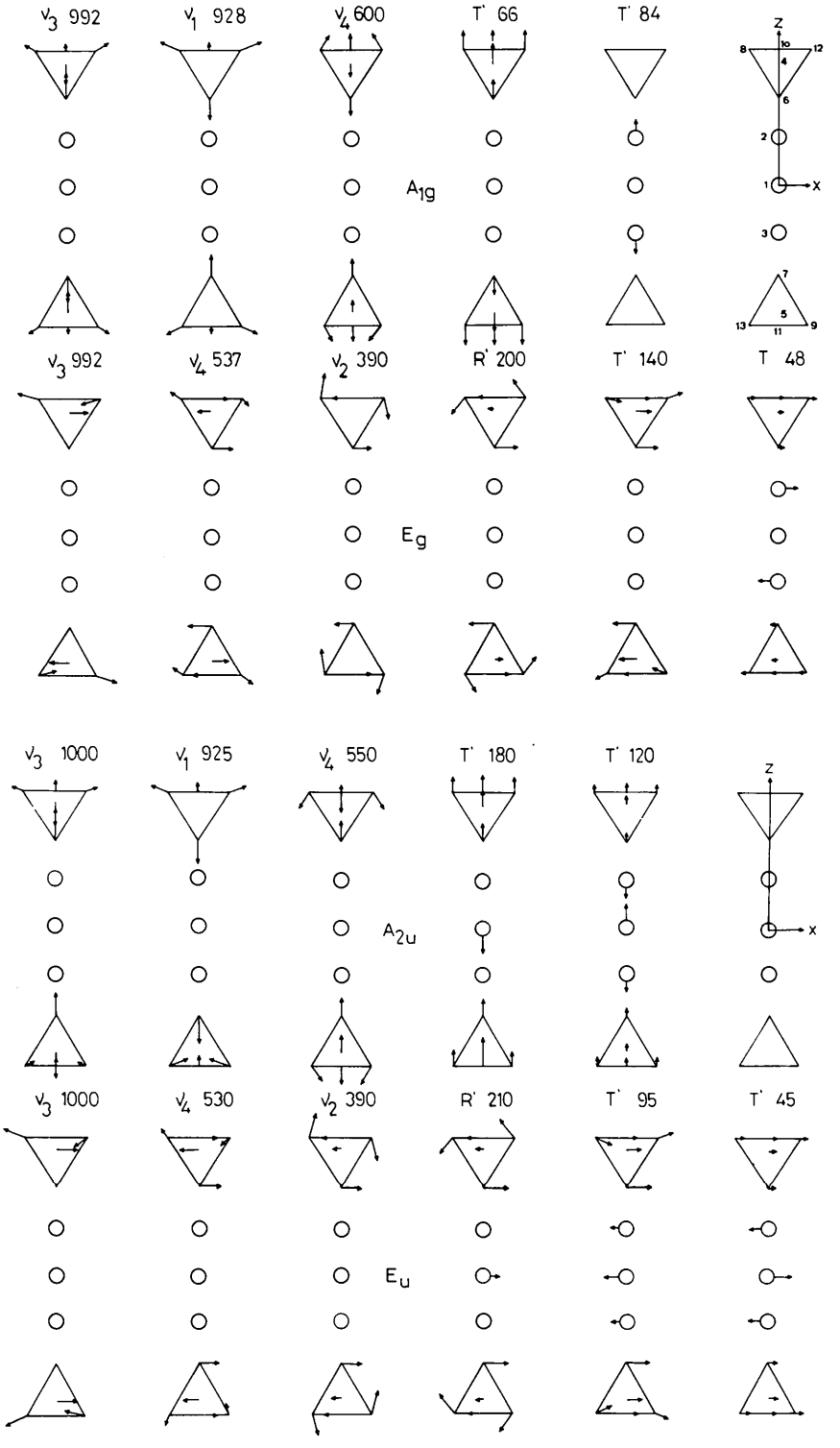

Fig. 9. Normal coordinates of trigonal $Pb_3(PO_4)_2$.

Discussion

The lattice-dynamical parameters with the strongest temperature dependence are the effective ionic charges. For $Pb_3(PO_4)_2$ and related mixed crystals the dynamical model shows a singularity induced by a small change of the ionic charge of Pb. The structural collapse is caused by the critical behaviour of the lowest-frequency phonon branch.

The changes of atomic positions during the transitions can be calculated if the phase relationship is known. From structural data the irreducible representation responsible for the high-temperature transition transforms according to the L point of the Brillouin zone. The amplitudes of the difference structure for the Pb atoms are parallel to the calculated normal coordinates and phase-shifted. The critical mode is a zone-boundary phonon. The ferroelastic behaviour is given by the geometrical distortion during the slowing down of this phonon. As three L points exist the wave vector will be parallel to one of them spontaneously. By external shear stress the three solutions can be transformed to each other as in the ferroelectric effect.

The swinging of both Pb positions is accompanied by slight rotation of PO_4 groups to reduce the Pb–O distance. The Madelung energy increases as the effective charges are relatively high for Pb and O.

The intermediate phase is characterized by strong internal stress observed in domain structures, phonon line broadening, and diffuse X-ray diffraction. From the critical behaviour of the L phonons for the two positions identical x and y parameters are required in the monoclinic phase. On the other hand the stable modification at low temperatures shows clearly different distances from the pseudo-hexagonal c_H axis for Pb(I) and Pb(II). Nevertheless the directions of the deformation vectors are still parallel. The transition between the intermediate phase and the low-temperature phase is of second order and is correlated with the critical behaviour of the same phonon branch as the first transition. The calculated normal coordinates of the critical phonon are in phase with the deformation vectors (at least for Pb). The absence of a strong dielectric anomaly demands a continuous character of the transition. All deformation vectors increase continuously with decreasing temperature. Simultaneously the dielectric constants decrease. From the LTSC relation,

$$\prod\left(\frac{\omega_L}{\omega_T}\right)^2 = \frac{\varepsilon_0}{\varepsilon_\infty} \quad (\approx 10 \text{ for } E_u \text{ modes}),$$

the slowing down of ω_T is related to the increase of static dielectric constant. The Kramers–Kronig analysis shows the low-frequency phonon branches as mainly responsible for ε_0. It is to be expected that the specific heat will increase with temperature.

The gradual transformation can be seen in the rotation of the magnetic axis (Ng & Calvo, 1975) in EPR experiments. The rotation angle decreases approximately linearly up to 160° and shows a force-field dependence in the intermediate phase. Here also the lower-temperature transition is more gradual and difficult to obtain.

To prove our theory, inelastic neutron scattering experiments measuring the frequency and dynamical coordinates of the L phonons near the point of the high temperature phase transition should be performed.

The crystals were grown by J. Tørres (Bagneux, France), K. Recker and collaborators (Bonn, Germany)

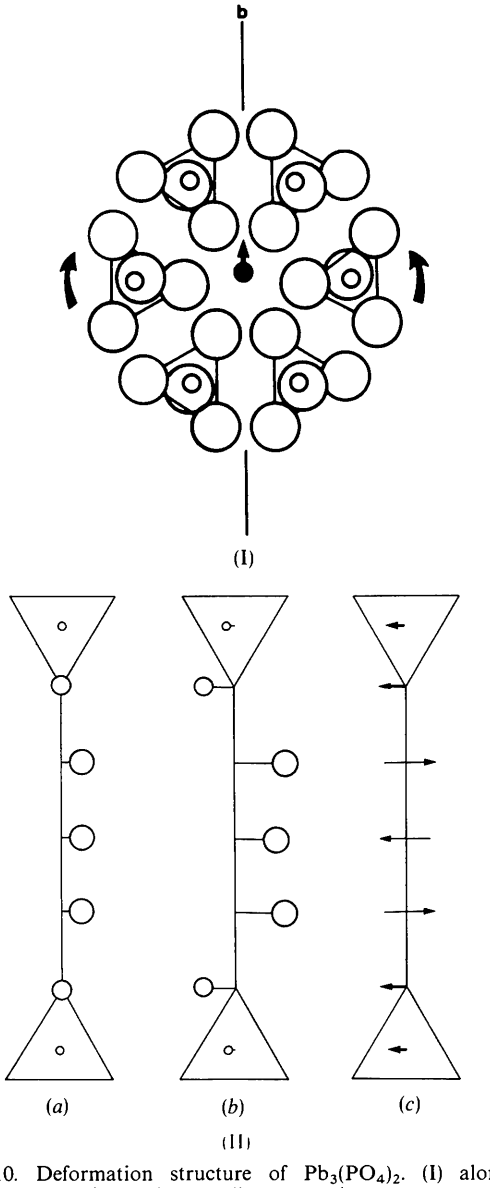

Fig. 10. Deformation structure of $Pb_3(PO_4)_2$. (I) along c_H, (II) along a_M in the intermediate (*a*) and room-temperature (*b*) phase. (*c*) denotes the difference vectors between the intermediate and low-temperature phase and represents the normal coordinates of the theoretical soft mode.

and R. von Hodenberg (Hannover, Germany). The authors are grateful for the use of these crystals. We are indebted to G. Hoppmann and U. Bismayer for technical assistance. The DFG has supported the Raman work. The infrared spectra were made with the instruments of the Chemical Institutes in Hannover.

References

BARAN, E. J., BOTTO, I. L. & AYMONINO, P. J. (1976). *Z. anorg. allgem. Chem.* **423**, 280–288.
BORN, M. & HUANG, K. (1954). *Dynamical Theory of Crystal Lattices*. Oxford: Clarendon Press.
BRIXNER, L. H., BIERSTEDT, P. E., JAEP, W. F. & BARKLEY, J. R. (1973). *Mater. Res. Bull.* **8**, 497–504.
CAO-XUAN, M. M., HAURET, G. & CHAPELLE, J. P. (1975). *C. R. Acad. Sci. Paris, sér. B*, **280**, 543–546.
EWALD, P. P. (1921). *Ann. Phys.* **64**, 253–287.
GENE, V. V., DUDNIK, E. F. & SINYAKOV, E. V. (1974). *Fiz. Tverd. Tela*, **16**, 3530–3532.
HODENBERG, R. VON, SALJE, E., RECKER, K., WALRAFFEN, F. & ECKSTEIN, J. (1977). To be published.
ISUPOV, V. A., KRAINIK, N. N. & KOSENKO, E. L. (1973). *Isv. Akad. Nauk. SSSR, Neorg. Mater.* **9**, 154–155.
KEPPLER, U. (1970). *Z. Kristallogr.* **132**, 228–235.
NG, H. N. & CALVO, C. (1975). *Canad. J. Phys.* **53**, 42–51.
SALJE, E. (1974). *Z. Kristallogr.* **139**, 317–334.
SALJE, E. & HOPPMANN, G. (1976). *Mat. Res. Bull.* **11**, 1545–1550.
SALJE, E. & VISWANATHAN, K. (1975). *Acta Cryst.* A**31**, 356–359.
SHIRO, Y. & MIYAZAWA, T. (1971). *Bull. Chem. Soc. Japan*, **44**, 2371–2378.
TØRRES, J. (1975). *Phys. Stat. Sol.* **b71**, 141–150.
TØRRES, J., AUBREE, J. & BRANDON, J. (1974). *Opt. Commun.* **12**, 416–417.

Acta Cryst. (1977). A**33**, 408–411

Long-Period Superstructure in Sodium–Lithium Metasilicates

BY A. R. WEST

Department of Chemistry, University of Aberdeen, Meston Walk, Old Aberdeen, Aberdeen AB9 2UE, Scotland

(*Received* 14 *October* 1976; *accepted* 26 *November* 1976)

The solid-solution series, high-$(Na_{2-x},Li_x)SiO_3$, $0{\cdot}86 \lesssim x \lesssim 1{\cdot}02$, has an orthorhombic subcell similar to the unit cells of Na_2SiO_3 and Li_2SiO_3 but with a one-dimensional long-period superstructure. The ratio $\kappa = a_{supercell}: a_{subcell}$ varies linearly with composition and integral κ values occur at simple Na:Li ratios: $\kappa = 6$ for 1Na:1Li ($x = 1{\cdot}00$) and $\kappa = 5$ for 5Na:4Li ($x = 0{\cdot}89$). Possible origins of the superstructure are discussed.

1. Introduction

During a study of the phase equilibria in the system Na_2SiO_3–Li_2SiO_3, a phase named high-$(Na,Li)_2SiO_3$ was encountered which apparently has a one-dimensional, long superstructure (West, 1976). This phase has a subcell similar to the unit cells of Na_2SiO_3 and Li_2SiO_3 (orthorhombic, space group $Ccm2_1$) but with extra X-ray reflexions on a^* such that $a_{supercell} = 6a_{subcell}$. Since simple Na/Li ordering would not normally be expected to give such a long-period superstructure, further study of this phase was felt to be worthwhile.

The phase diagram of the Na_2SiO_3–Li_2SiO_3 system is known (West, 1976). Both Li_2SiO_3 and Na_2SiO_3 form a range of equilibrium solid solutions (s.s.), and the Na_2SiO_3 solid solutions are particularly extensive at solidus temperatures, covering just over half of the diagram at about 850 °C. Although the equilibrium phase diagram is simple, complexities arise during cooling of the Na_2SiO_3 solid solutions; they are associated with the occurrence of metastable phases and reactions. In the region of interest to this paper, around the 1:1 composition $(Na,Li)_2SiO_3$, the Na_2SiO_3 s.s. phase is stable only above about 810 °C; at all temperatures below this, two phases coexist at equilibrium. However, single-phase products may be retained metastably to room temperature by quenching from above 810 °C. With rapid quenching (~1 s; samples dropped into Hg), the high-$(Na,Li)_2SiO_3$ phase forms; this phase is apparently similar to the high-temperature Na_2SiO_3 s.s., but in addition has an X-ray superstructure. With somewhat slower cooling rates (~20 s; samples cooled in air), low-$(Na,Li)_2SiO_3$ forms: this phase is a monoclinic distortion of the orthorhombic high-temperature solid solution and does not have a superstructure. High-$(Na,Li)_2SiO_3$ may be converted to low-$(Na,Li)_2SiO_3$ by annealing at 400–500 °C and low-$(Na,Li)_2SiO_3$ may be decomposed into the equilibrium, low-temperature assemblage, (Na_2SiO_3 s.s. + Li_2SiO_3 s.s.), by heating at 600–700 °C.

2. Experimental

Bulk preparations (about 10 g) of metasilicate compositions were prepared by reaction in Pt crucibles in electric muffle furnaces of appropriate quantities of Na_2CO_3, Li_2CO_3 (both reagent grade) and SiO_2 (crushed natural quartz crystal), initially at about